Journal of Applied Physics

Non-steady state transport of charge carriers. An approach based on invariant embedding method

Cite as: J. Appl. Phys. **127**, 045703 (2020); https://doi.org/10.1063/1.5136090
Submitted: 11 November 2019 . Accepted: 07 January 2020 . Published Online: 22 January 2020

C. Figueroa, B. Straube, M. Villafuerte, G. Bridoux, J. Ferreyra, N. C. Vega, and S. P. Heluani

View Online

Export Citation

CrossMark

ARTICLES YOU MAY BE INTERESTED IN

Nanoscale electro-thermal interactions in AlGaN/GaN high electron mobility transistors
Journal of Applied Physics **127**, 044502 (2020); https://doi.org/10.1063/1.5123726

Improving the performance of light-emitting diodes via plasmonic-based strategies
Journal of Applied Physics **127**, 040901 (2020); https://doi.org/10.1063/1.5129365

Identification of the donor and acceptor states of the bond-centered hydrogen–carbon pair in Si and diluted SiGe alloys
Journal of Applied Physics **127**, 045701 (2020); https://doi.org/10.1063/1.5135757

© 2020 Author(s).

Journal of Applied Physics | ARTICLE | scitation.org/journal/jap

Non-steady state transport of charge carriers. An approach based on invariant embedding method

Cite as: J. Appl. Phys. **127**, 045703 (2020); doi: 10.1063/1.5136090
Submitted: 11 November 2019 · Accepted: 7 January 2020 ·
Published Online: 22 January 2020

C. Figueroa,[a] B. Straube, M. Villafuerte, G. Bridoux, J. Ferreyra, N. C. Vega, and S. P. Heluani

AFFILIATIONS

Facultad de Ciencias Exactas y Tecnología, Laboratorio de Física del Sólido, INFINOA (CONICET-UNT), Universidad Nacional de Tucumán, 4000 San Miguel de Tucumán, Argentina

[a]**Author to whom correspondence should be addressed:** cfigueroa@herrera.unt.edu.ar

ABSTRACT

In this work, we report on a model that describes the microscopic electrical transport as a transmission problem using the invariant embedding technique. Analytical expressions for the transport coefficients under non-steady-state conditions are derived allowing us to calculate carrier concentration and time-dependent conductivity. Employing measurable magnitudes, our theoretical results allow us to determine defect concentrations, carrier generation rates, cross sections of recombination, and capture by traps. This model can be employed to study the conduction processes of semiconductors and test their band and defect structure. In particular, time-dependent photoconductivity measurements of a ZnO microwire have been well fitted using our model indicating a relevant role of intrinsic point defects in this material.

Published under license by AIP Publishing. https://doi.org/10.1063/1.5136090

I. INTRODUCTION

Theoretical understanding of non-steady-state transport properties of optically active semiconductors has received relatively less attention despite the wide experimental activity in the field. Nowadays, most of these experiments are described by empirical or semiempirical models, as the multiple trapping model[1,2] or by simulations[3] and numerical solutions (i.e., the donor photoionization model[4]). However, a few theoretical efforts using first principles were reported; the most prominent one is due to DeVore,[5] where surface effects and volume recombination of photocarriers have been considered for a particular set of boundary conditions. Ullrich and Xi[6] improved this model arguing that the boundary conditions adopted in DeVore's transport equations are not consistent with the typical experimental conditions. On the other hand, an application of adequate boundary conditions to Boltzmann's equation is particularly hard in semiconductor oxides under spatially inhomogeneous charge distributions, due to the presence of adsorbate-induced surface doping, band bending, etc.[7] An alternative formalism to describe transport phenomena is the Invariant Embedding Method (IEM) first described by Ambarzumian[8] in the context of atmospheric scattering problems and then used in several physical processes.[9–12] The IEM provides first order-differential equations subject only to initial conditions in space and time coordinates in contrast to the traditional nonlinear transport equations with boundary conditions.[13–15] This method allows one to obtain differential equations and analytical expressions for transport coefficients of particle fluxes with different trajectories (or "destinations") inside a solid sample, considering one of the system dimensions as the independent variable. Inspired on the Landauer formalism for a mesoscopic system,[16] we apply IEM procedures to study non-steady-state transport phenomena in semiconductors. As a proof of the validity of our model, we have fitted the time-dependent photoconductivity measurements on a ZnO microwire using our theoretical approach. These data are divided into three stages: (1) *Pre-excitation*: conductivity response in the dark to the drop of ambient pressure due to the release of surface oxygen. (2) *Excitation*: growth of conductivity under UV illumination. (3) *Recuperation*: decay of conductivity after turning the UV irradiation off. From the fits, we obtain a set of physical parameters of the sample in agreement with the ones reported in the literature.

Published under license by AIP Publishing.

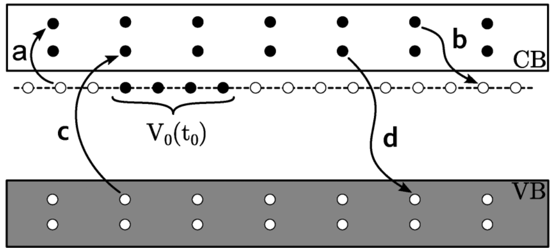

FIG. 1. The scheme shows a simple band structure proposed for a semiconductor. The processes considered in the model are: (a) electron release from a donor impurity to CB, (b) CB electron capture by donor impurity acting as an electron trap, (c) electron–hole (e)–(h) pair photogeneration, and (d) electron–hole recombination. $V_o(t_0)$ indicates the initial concentration of neutral defects. Black circles indicate electrons and white ones, holes.

II. INVARIANT EMBEDDING METHOD (IEM)

In this section, we describe the general procedure to apply the IEM to a carrier transport problem in a semiconductor sample.

A. Basic processes and transport coefficients for a simple model

First, we propose a simple model for the band structure of a semiconductor, and then, we enumerate the principal processes that can occur as the carriers pass through the sample.

Consider an ideal semiconductor material with high crystallinity, low charge carrier concentration, and a concentration of donors, ρ. An external voltage is applied across the sample of length L and is simultaneously excited by an adequate radiation. Let us call $V_o(t_0)$, the initial concentration of neutral defects; n_0 and p_0 are the initial concentration of free electrons in the Conduction Band (CB) and holes in the Valence Band (VB), respectively. The processes considered here are shown in Fig. 1. For simplicity, both types of carriers have the same drift velocity, v_d. Then, we assume that the change of conductivity is attributable only to the change in the charge carrier concentrations.

Figure 2 shows the basic paths for carriers passing through the sample and their respective transport coefficients. The net increase or decrease of carrier densities depends on the balance between generation or absorption of e-h pairs and on the capture and release of electrons by traps. Processes labeled as (3)–(7) effectively contribute to measurable electrical current in the external circuit. Processes (1) and (6) change the ionization rate of defects.

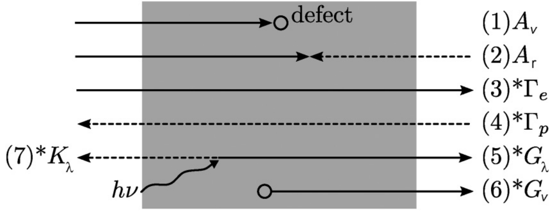

FIG. 2. The scheme shows the basic paths of the carriers as passing through the sample. Full lines indicate the trajectory of electrons, while dotted lines indicate the trajectory of holes. The asterisk marks the process that contributes to the initial current in the next step ($t+\tau$) (see the text).

The interval of time that we use in our procedure as a "step time" is the transit time, $\tau = \frac{L}{v_d}$. During this interval of time, the net change of the electron and hole densities is

$$\Delta n = n_0\,\Gamma_e + G_\lambda + G_v, \tag{1}$$

$$\Delta p = p_0\,\Gamma_p + K_\lambda, \tag{2}$$

where Γ_e and Γ_p are the electron and hole transmission coefficients, respectively. G_λ and K_λ are the electron and hole photogeneration coefficients, respectively, and G_v is the coefficient of electron release by traps.

In Fig. 2, processes (1) and (2) denoted as A_v and A_r, are the electron capture and the e-h recombination coefficients, respectively. On the other hand, during the transit time τ, an amount $A_r\,n_0$ of electrons will recombine with holes. The net change of neutral vacancy concentration per time interval τ is

$$\Delta V_0 = A_v\,n_0 - G_v. \tag{3}$$

B. Calculus of the electron photogeneration coefficient (G_λ) using IEM

As an illustration of the IEM, we describe in this subsection the procedure to obtain the differential equation for the transport coefficient, G_λ, and its solution. The rest of the coefficients can be evaluated using the same procedure.

We recall that G_λ evaluates the increment in the electron concentration in a time interval τ. The typical procedure in IEM is to take the sample thickness as the integration variable in the differential equations for probabilities. In this scheme, dG_λ is the differential increase of $G_\lambda(L)$ corresponding to a differential increase of length, dL. Photogenerated electrons that reach the end of the sample contribute to the final electron current density. Using the usual procedure, at the end of the sample, we add a differential layer dL (see Fig. 3) and then proceed to evaluate $G_\lambda(L+dL)$,

$$G_\lambda(L+dL) = G_\lambda(L)(1 - s dL) + g_\lambda dL, \tag{4}$$

where s is the probability of absorption of electrons and g_λ is the factor of photogeneration, both per unit length in a time interval τ. The first term in the right side of Eq. (4) is the probability of generating an electron in the sample of size L, $G_\lambda(L)$, multiplied by the probability that it passes through the layer dL without suffering absorption and leaving the sample at the end. The second term is the probability that an electron photogenerated

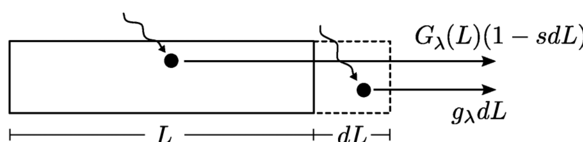

FIG. 3. Probable paths of photogenerated electrons in a sample of length "$L + dL$."

Published under license by AIP Publishing.

inside the layer dL leaves the sample at the end. Using Eq. (4) is straightforward to obtain

$$\frac{dG_\lambda(L)}{dL} = sG_\lambda(L) + g_\lambda, \tag{5}$$

$$G_\lambda(L) = \frac{g_\lambda}{s}\,(1 - \exp(-s\,L)). \tag{6}$$

Then, $G_\lambda(L)$ is used to calculate the change of carrier density due to the electron photogeneration in each interval τ, and its units will be (particles/cm^3). Thereby, the units of factor g_λ will be particles/cm^4. Here, it is necessary to clarify that although the coefficients are deduced as functions of L, it is obvious that the sample length is not a variable. Instead, these functions depend on factors such as g and s, which, in turn, depend on time, so the coefficients are function of time. For simplicity, we will express the coefficients as a function of its characteristic factors as $G_\lambda(g_\lambda, s)$.

C. Expressions for the coefficients related to generation and absorption

Using a similar procedure as the one used to calculate the $G_\lambda(L)$ coefficient in Sec. II B, we can calculate the absorption coefficients: A_v and A_r, and the generation coefficients: G_v and K_λ. The transmission coefficients will be calculated in Sec. II D.

Electron capture by impurities:

$$A_v(s, s_v) = s_v\left(\frac{sL - 1 + \exp(-sL)}{s^2 L}\right). \tag{7}$$

Electron–hole recombination:

$$A_r(s, s_r) = s_r\left(\frac{sL - 1 + \exp(-sL)}{s^2 L}\right). \tag{8}$$

Electron release by impurities:

$$G_v(g_v, s) = \frac{g_v}{s}(1 - \exp(-sL)). \tag{9}$$

Hole photogeneration:

$$K_\lambda(g_\lambda, s_p) = \frac{g_\lambda}{s_p}(1 - \exp(-s_p L)), \tag{10}$$

where s_r and s_p are the *probabilities of recombination for electrons* and *holes*, respectively. s_v is the *probability of capture of electrons*. Then, $s = s_r + s_v$ is the total probability of absorption of electrons. g_v is the *rate at bulk trap release electrons*. All these probabilities are per unit length.

In the previous scheme, two processes were neglected, one is that an electron is photogenerated and captured by a trap, $A_{\lambda v}$, and the other is that an electron released by a trap recombines with a hole, B_{vr}, both cases within the time interval τ. If these processes are appreciable, the following cross coefficients must be added:

$$A_{\lambda v}(g_\lambda, s, s_v) = \frac{g_\lambda s_v}{s^2}\,(\exp(-s\,L) + sL - 1), \tag{11}$$

$$B_{vr}(g_v, s, s_r) = \frac{g_v s_r}{s^2}\,(\exp(-s\,L) + sL - 1). \tag{12}$$

D. Transmission coefficients

Consider an initial concentration of CB electrons n_0, at time t_0, that passes through a sample of volume V as previously described. If the medium absorbs particles with a probability s per unit length, the total number of carriers $N_1 = n_1 V$ reaching the end of the sample and, therefore, that contribute to the electrical current in the next step at time $t_0 + \tau$ will be

$$N_1 = \Gamma_e\, n_0\, V = n_0\, A \int_0^L e^{-xs} dx = n_0\, A(1 - e^{-Ls})/s, \tag{13}$$

where x is the coordinate along the sample and A is the sample cross section. We can express

Transmission coefficient for electrons

$$\Gamma_e(s) = \frac{1 - \exp(-L\,s)}{L\,s}, \tag{14}$$

Transmission coefficient for holes

$$\Gamma_p(s_p) = \frac{1 - \exp(-s_p L)}{s_p L}. \tag{15}$$

It is worth remarking that unlike the generation coefficients, the transmission, absorption and cross coefficients are dimensionless. The latter three express the fraction of the total number of carriers that have different destinations at each step τ. The picture described here has the advantage of great explanatory power, but its inconvenience is that transport coefficients are not normalized in seconds. However, this problem is solvable under the assumption that there is no appreciable change in the charge concentration during any other time interval greater than τ. Under this condition, there is a direct linear relationship between non-normalized and normalized probabilities per unit of time and length.

E. Electrodynamical consistency of the transport equations

In order to ensure the electrodynamical consistency of the equations, charge conservation and uniform carrier density throughout the sample are necessary conditions. In this picture, charge carrier's density in both bands are uniform in space because they are delivered (or extracted) with space independent rates (g or s) in such a way that the probability of absorption or generation of carriers is the same along the sample. Carriers reaching the end of the sample contribute to measurable current. The continuous temporal changes of electrical transport parameters are represented by a quasistatic process, a succession of steady state steps that preserve the form of electrical transport equations.

III. APPLICATION TO A REAL CASE: ZINC OXIDE MICROWIRE

We will apply the procedure described in Sec. II to fit the time-dependent conductivity measured in a ZnO microwire using a

Published under license by AIP Publishing.

simplified band and defect structure model. We choose this material to apply the IEM because it has persistent photoconductivity.

A. Experimental details and measurement results

The sample measured is a ZnO microwire (MW) of length $L = 125\,\mu$m and diameter $\phi = 55\,\mu$m. For details of fabrication and characterization, see Refs. 17 and 22. Ohmic electrical contacts were made with indium soldering for conductivity measurements. An excitation voltage of 5 V was used, and the electrical current was measured with a resolution of 0.5 nA. Measurements were carried out at room temperature in a standard cryostat equipped with an optical window and a 1000 W Xe lamp plus a Oriel monochromator with an estimated flux density of $10\,\mu$W cm^{-2} in the UV range. The wavelength of the light used for excitation was 370 nm. Before the measurement, the sample was kept in the dark at ambient pressure for 24 h.

Figure 4 shows the result of the variation of the conductivity with time for the three stages, where the conductivity was normalized using the value, $\sigma_0 = 1.75 \times 10^{-4}\,\Omega^{-1}\,\mathrm{cm}^{-1}$. This value was obtained from $R_0 = 3.0 \times 10^6\,\Omega$, the final value of equilibrium in vacuum and dark and an electron mobility[28] $\mu_e = 205\,\mathrm{cm}^2/\mathrm{V\,s}$. The corresponding carrier concentration is $n_0 = 5.34 \times 10^{12}\,\mathrm{cm}^{-3}$, which is expected for a highly crystalline sample with low defect concentration. Also, the carrier concentration will be normalized using this value.

In the first stage, that we call the *pre-excitation stage*, the vacuum pump was turned on with the sample still in the dark. After 2.4×10^4 s ($\approx$6.7 h), the sample appears to reach a stable conductivity value. At this time, the *excitation stage* starts when the UV lamp is turned on, during this stage, the conductivity grows approximately five times. At 8.2×10^3 s ($\approx$2.3 h), the UV lamp is turned off and the *recuperation stage* begins. We measured the conductivity for around 8.4×10^4 s ($\approx$23.3 h), until it approximates the initial value of the excitation stage.[17,27]

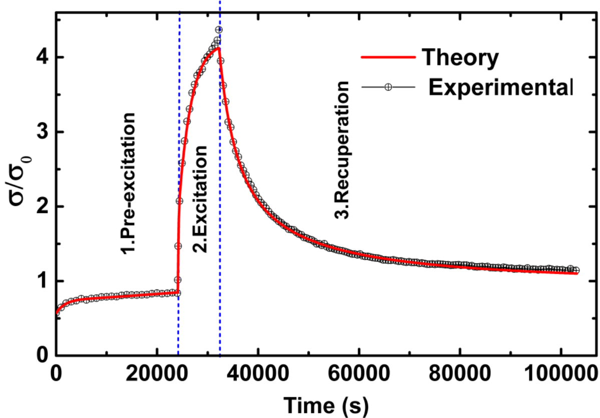

FIG. 4. Variation of normalized conductivity of ZnO microwire in the three stages. The stage of excitation starts at 24 000 s and the recuperation one starts at 32 200 s. The theoretical curve is in red, experimental one in black.

B. Model for the defect energy levels of the ZnO microwire

In order to apply the IEM to explain and fit the behavior of the photoconductivity of the MW, it is necessary to assume a model for the energy level of defects present in the band structure. Based on the literature on defects in ZnO,[17,18,21,26,28] we assume three types of defects: (i) bulk oxygen vacancies of concentration ρ, (ii) surface oxygen vacancies of variable concentration, and (iii) a concentration, ζ, of defects with energies closer to the VB top, that act as hole traps[18] (see Fig. 5).

In the stage of *pre-excitation*, the initial conductivity of the sample is due to electrons present in the CB due to the thermal ionization of bulk oxygen vacancies.[21–26] In this stage, we observe an increase of conductivity in the dark. Our model attributes this change in the conductivity to the generation of surface oxygen vacancies.[19,20] Let us consider that each surface oxygen is linked to two zinc atoms by two-electron bonding. When a surface oxygen is released, a surface vacancy is formed with two electrons in energetically shallow levels. Then, these levels deliver electrons to the CB, producing the change in conductivity on time. The degree of surface oxidation falls from the equilibrium value corresponding to ambient pressure to a new equilibrium value corresponding to the final vacuum pressure.

In the *excitation stage*, the sample is irradiated with UV light, pumping electrons from the VB to the CB, supplying charge carriers to both bands. In this stage, we assume that the surface was completely deoxidized in the previous stage, so we neglect the change of the surface oxygen concentration. A higher concentration of free electrons and holes will cause a competition between e-h recombination and UV generation of these carriers. We will consider e-h recombination only as a direct band to band process. Also, we assume a negligible exciton lifetime, so the effect of excitons in the whole process will not be taken into account. Additionally, the UV light ionizes the hole traps, pumping electrons directly to CB (see Fig. 5). Besides, the hole traps can be ionized by the thermal effect, trapping a VB hole, or can be neutralized by releasing one. Then, the effective concentration of charge carriers in both bands is determined by the exchange of particles between both bands and with another two *reservoirs*: the bulk oxygen vacancies and the hole

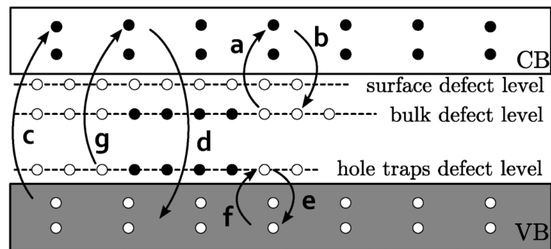

FIG. 5. Transitions considered in the stage of excitation: (a) electron release by donor neutral levels, (b) electron capture by donor ionized levels, (c) e-h pair generation, (d) e-h recombination, (e) hole release by acceptor ionized levels, (f) hole capture by acceptor neutral levels, and (g) UV ionization of acceptor neutral levels.

Published under license by AIP Publishing.

traps. Under the action of the UV light, these four *reservoirs* will tend to a new dynamical equilibrium with a higher density of electrons and holes in the bands and a higher rate of ionization of defects than in the dark.

After turn off the UV light, i.e., during *recuperation* stage, the transport process is dominated by the trend of the whole system to the equilibrium state in the dark. In this way, the ionization rate of bulk oxygen vacancies and hole traps tend to recuperate its dynamical thermal equilibrium, and the recombination between electrons and holes decreases the charge carriers density in both bands. This process continues until VB holes disappear and CB electron density recuperates its "thermal level." In this model, we include the different mobility of electrons and holes by means of an adjustable parameter $f = \frac{\mu_p}{\mu_e}$ (where μ_p is the VB hole mobility), then the conductivity is calculated as $\sigma(t) = [n(t) + f\,p(t)]\,e\mu_e$. Finally, changes in the temperature of the sample due to the Joule effect are neglected in all stages.

C. Fitting the data using IEM coefficients

The model established in Sec. III B provides a preliminary explanation of the time-dependent conductivity for the three stages at room temperature. The physical parameters such as CB electron density $n(t)$, VB hole density $p(t)$, concentration of neutral and ionized defects, and conductivity $\sigma(t)$ will be calculated as a function of time by means of **iterations**. The fitting was designed to adjust simultaneously all three stages using *lmfit* package from Python[29] with 15 parameters. For convenience, we take the iteration step as $\tau_{step} = 1$ s, thereby all parameters and coefficients will be defined in seconds, under the assumption that, during the interval $\tau_{step} = 1$ s, the change in the carrier's concentration is neglectable and thereby the transport coefficient expressions are applicable.

Iterative calculations for stage of pre-excitation:

During the pre-excitation process, the normalized electron concentration changes from the initial value $n_i = 0.572$ until the final value $n_0 = 1$ (calculated from the data of Fig.5). We attribute this difference to the electrons provided by surface deoxidation, then the change of conductivity is governed by the deoxidation rate. Here, we assume the condition $p(t) = 0$ over this period of time.

The following expressions will be iterated, where for simplicity, the coefficients are expressed as a function of time:

$$n(t + \tau_{step}) = \Gamma_e(t)\, n(t) + G_s(t) + G_v(t), \tag{16}$$

$$S_o(t + \tau_{step}) = S_o(t) - G_s(t) - A_{sv}(t) + A_s(t)\, n(t) + 2\,\frac{d\xi}{dt}\,\tau_{step}, \tag{17}$$

$$V_o(t + \tau_{step}) = V_o(t) - G_v(t) + A_v(t)\, n(t) + A_{sv}(t). \tag{18}$$

In the right member of Eq. (16), we consider the transmitted electrons [Eq. (14)] plus the electrons released by bulk traps [Eq. (9)], and we add the *electrons released by oxygen surface vacancies,*

$$G_s(g_s, s) = \frac{g_s}{s}(1 - \exp(-sL)). \tag{19}$$

Here, $S_o(t)$ [Eq. (17)] stands for the neutral surface vacancy concentration, where $A_{sv}(t)$ is the cross coefficient due to *exchange of electrons from surface to bulk vacancies,*

$$A_{sv}(g_s, s, s_v) = \frac{g_s s_v}{s^2}\,(\exp(-s\,L) + sL - 1), \tag{20}$$

Here, $A_s(t)$ is the *electron capture by oxygen surface vacancies,*

$$A_s(s, s_s) = s_s\left(\frac{sL - 1 + \exp(-sL)}{s^2 L}\right). \tag{21}$$

Also, the term $2\,\frac{d\xi}{dt}\,\tau_{step}$ is the surface vacancy concentration (two per atom) generated in the iteration step τ_{step}. We propose the following function of time for the *surface oxygen vacancy concentration*:

$$\xi(t) = \xi_0\left[1 - c\,\exp\left(-\frac{t}{\tau_1}\right) - (1 - c)\,\exp\left(-\frac{t}{\tau_2}\right)\right], \tag{22}$$

where ξ_0=0.4246. Finally, Eq. (18) for $V_o(t)$ calculates the neutral bulk vacancy concentration as a function of time.

The probabilities that involve the latter coefficients are defined as

$$s_v(t) = k_v\;(\rho - V_o(t)), \tag{23}$$

$$s_s(t) = k_s\,(2\xi(t) - S_o(t)), \tag{24}$$

$$g_s(t) = b_s(2\delta_c - n(t))S_o(t), \tag{25}$$

$$g_v(t) = b_v(2\delta_c - n(t))V_o(t), \tag{26}$$

where s_v depends on simply ionized vacancy concentration, $\rho - V_o(t)$ (ρ is the total oxygen vacancy density) and s_s depends on the concentration of ionized surface oxygen vacancies $2\xi(t) - S_o(t)$. As an example, the constant k_v is

$$k_v = \frac{\mathbf{v}\,\chi_v\,n_0\,\tau_{step}}{L}, \tag{27}$$

where χ_v is the cross section of capture of the bulk traps and $\mathbf{v}$ is the velocity of carriers. g_v and g_s depends on the respective concentration of neutral oxygen vacancies and the density of available states in the CB: $2\delta_c - n(t)$, where δ_c is the effective density of electron states in the CB.

Expressions for excitation and recuperation:

In the stage of excitation, it is possible to determine the CB electron density, $n(t)$, the neutral bulk oxygen defect concentration, $V_o(t)$, the VB hole density $p(t)$ and the ionized hole trap concentration, $V_z(t)$. The expressions used for iteration are

$$p(t + \tau_{step}) = \Gamma_p(t)p(t) + K_\lambda(t) + K_z(t) - B_{\lambda r}(t) - B_{vr}(t) - B_{\mu r}(t), \tag{28}$$

$$n(t + \tau_{step}) = \Gamma_e(t)n(t) + G_\lambda(t) + G_v(t) + G_\mu(t) - A_{\lambda r}(t) - A_{zr}(t), \tag{29}$$

Published under license by AIP Publishing.

$$V_o(t+\tau_{step}) = V_o(t) - G_v(t) + A_v(t)n(t) + A_{\lambda v}(t) - B_{vr}(t) + A_{\mu v}(t), \quad (30)$$

$$V_z(t+\tau_{step}) = V_z(t) + G_\mu(t) - K_z(t) + B_z(t)p(t) - A_{zr}(t) + B_{\lambda z}(t) + B_{\mu r}(t) + A_{\mu v}(t). \quad (31)$$

The additional coefficients, besides $\Gamma_p(s_p)$, which were previously defined in Eq. (15), are the following:

Hole capture by traps: $B_z(s_z, s_h) = s_z\left(\frac{s_h L - 1 + \exp(-s_h L)}{s_h^2 L}\right).$

Trap capture of holes photogenerated in the interval τ_{step}:

$$B_{\lambda z}(g_\lambda, s_h, s_z) = \frac{g_\lambda s_z}{s_h^2}\,(\exp(-s_h\, L) + s_h L - 1).$$

Electron generation : $G_j(g_j, s) = \frac{g_j}{s}(1 - \exp(-s\, L)).$

Hole recombination with electrons generated in the interval τ_{step}:

$$B_{jr}(g_j, s, s_r) = \frac{g_j s_r}{s_h^2}\,(\exp(-s_h\, L) + s_h L - 1)$$

Hole generation: $K_i(g_i, s_h) = \frac{g_i}{s_h}(1 - \exp(-s_h L)$

Electron recombination with holes generated in the interval τ_{step}:

$$A_{ir}(g_i, s_h, s_p) = \frac{g_i s_p}{s_h^2}\,(\exp(-s_h\, L) + s_h L - 1).$$

Vacancy capture of electrons generated in the interval τ_{step}:

$$A_{kv}(g_k, s, s_v) = \frac{g_k s_v}{s_h^2}\,(\exp(-s_h\, L) + s_h L - 1),$$

with $j = \lambda, v, \mu$, $i = \lambda, z$, and $k = \lambda, \mu$, where λ refers to electrons and holes photogenerated, v to electrons released by oxygen vacancies, μ by hole trap photoionization, and z refers to holes thermically released by traps.

The corresponding probabilities for the coefficients are

$$s_p(t) = \kappa n(t), \quad (32)$$

$$s_r(t) = \kappa\, p(t), \quad (33)$$

$$s_z(t) = k_z\,(\zeta - V_z(t)), \quad (34)$$

$$g_v(t) = b_v(2\delta_c - n(t))V_o(t), \quad (35)$$

$$g_z(t) = b_z(2\delta_v - p(t))V_z(t), \quad (36)$$

$$g_\lambda(t) = \lambda(2\delta_c - n(t))(2\delta_v - p(t)), \quad (37)$$

$$g_\mu(t) = b_\mu(2\delta_c - n(t))(\zeta - V_z(t)). \quad (38)$$

with $s_h = s_p + s_z$ and $s = s_r + s_v$. Here, s_z is the probability per unit length of hole capture by a trap that depends on $\zeta - V_z(t)$ (neutral trap concentration). g_λ, g_μ, and g_z are the rates per unit length of generation of hole-electron pairs, trap ionization, and hole release by neutral traps, respectively. Figure 4 shows the result of the fitting of the experimental values of the normalized conductivity for the three stages. Table I shows the values of the fitted parameters.

TABLE I. The 15 fitted parameters.

$c = 0.213$	
$\tau_1 = 2326.8$ s	Deoxidation function constants
$\tau_2 = 29\,623$ s	
$\rho = 14.29$	Normalized density of oxygen vacancies
$\zeta = 0.913$	Normalized density of hole traps
$K_v = 1.296$	Unitary probability of electron capture by a bulk oxygen vacancy
$K_z = 4.08$	Unitary probability of hole capture by a trap
$\lambda = 1.54 \times 10^4$	Photocarrier generation efficiency
$b_z = 8.86 \times 10^4$	Hole trap ionization efficiency
$b_\mu = 4.7 \times 10^6$	Bulk oxygen vacancy ionization efficiency
$b_s = 3.67 \times 10^8$	Surface oxygen vacancy ionization efficiency
$f = 0.127$	Electron–hole mobility relation
$\kappa = 0.57$	Unitary probability of electron–hole recombination
$\delta_c = 19.79$	Effective normalized density of BC electron states
$\delta_v = 26.77$	Effective normalized density of BV electron states

D. Characteristic parameters obtained from the fitted values

The procedure presented in this work serves for the determination of characteristic transport parameters of a particular material. In this case, some of the fitted parameters converted to the values with their corresponding units are shown below:

- *Oxygen vacancy concentration*: $\rho = 7.62 \times 10^{13}$ cm^{-3}.
- *Neutral oxygen vacancy density* (thermal value at room temperature and vacuum): $V_o(t_0) = 7.1 \times 10^{13}$ cm^{-3}.
- *Hole trap defect concentration*: $\zeta = 4.88 \times 10^{12}$ cm^{-3}.
- *Effective energy state density in the CB*: $\delta_c = 5.28 \times 10^{13}$ cm^{-3}.
- *Effective energy state density in the VB*: $\delta_v = 7.95 \times 10^{13}$ cm^{-3}.
- *Surface oxygen vacancy density* corresponding to the maximum oxidation: $\xi_0 = 2.267 \times 10^{14}$ cm^{-2}.

Using these values, it is possible to obtain parameters related to the efficiency of the traps,

- *Recombination cross section for electrons*: $\chi_e = 5.67 \times 10^{-25}$ cm^2.
- *Recombination cross section for holes*: $\chi_p = 8.7 \times 10^{-25}$ cm^2.
- *Vacancy capture cross section for electrons*: $\chi_v = 1.29 \times 10^{-24}$ cm^2.
- *Trap capture cross section for holes*: $\chi_z = 6.29 \times 10^{-24}$ cm^2.
- *Hole mobility*: $\mu_p = 0.127\mu_e$.

In relation to bulk oxygen vacancies, we have considered a unique level (1st level of oxygen vacancies), whose energy is about 0.88 eV below the CB minimum.[23] Considering this energy level and the value $V_o/\rho = 0.93$ obtained in the present work, it is possible to estimate the Fermi level using $f(E_d) = \frac{V_o}{\rho} = \left(1 + g\,\exp\frac{E_d - E_f}{k_b T}\right)^{-1}$

Published under license by AIP Publishing.

with $g = 1/2$ for ZnO[30] at room temperature. Our calculation predicts a value for E_f of 0.93 eV, below the CB minimum.

The results obtained in this work are strongly dependent on the value used for electron mobility. This value determines the density of carriers and, therefore, the remaining parameters. However, the estimated concentration of defects (oxygen vacancies and hole traps) is consistent with the initial hypothesis of high crystallinity and low density of charge carriers for the ZnO MW. In the case of capture cross sections, the values found in the literature vary up to 12 orders of magnitude. Such dispersion is indicative of the approximate and indirect nature of the methods used to determine this parameter. The values obtained in this work are halfway within the range covered by previous estimates.[31,32]

The parameters related to the generation of photoelectrons will be subject to further analysis in the future work.

E. Population of bands and concentration of ionized traps

Figure 6 shows the temporal variation of hole and electron concentration at the three stages. The CB electron concentration, corresponding to thermal equilibrium, at room temperature and vacuum pressure, is indicated by the horizontal line. During the process of recuperation, the CB electron concentration asymptotically tends to $n_0 = 1$, while the VB hole concentration, which is considered negligible in the first stage, falls asymptotically to zero. Also, we can evaluate the rate of vacancy ionization or the concentration of neutral vacancies during the different stages. Figure 7 shows the variation of neutral vacancy concentration $V_o(t) - V_o(t_o)$ and the variation of ionized hole trap concentration, $V_z(t)$ for the whole process. The reference value corresponding to thermal equilibrium concentration is marked by the horizontal line. When UV light is turned on, the concentration of neutral vacancies and electrons in the CB grow above their thermal level. When UV light is turned off, the e-h generation stops but the concentration of electrons in CB falls off slowly since the neutral vacancies start to release electrons slowly to the CB to reach their thermal level concentration. On the other hand, UV excitation causes the ionization of the defects that act as hole traps, capturing holes. Both phenomena retain charge carriers from both bands, and when excitation ceases, they release the charge carriers with their characteristic time delaying the e-h recombination.

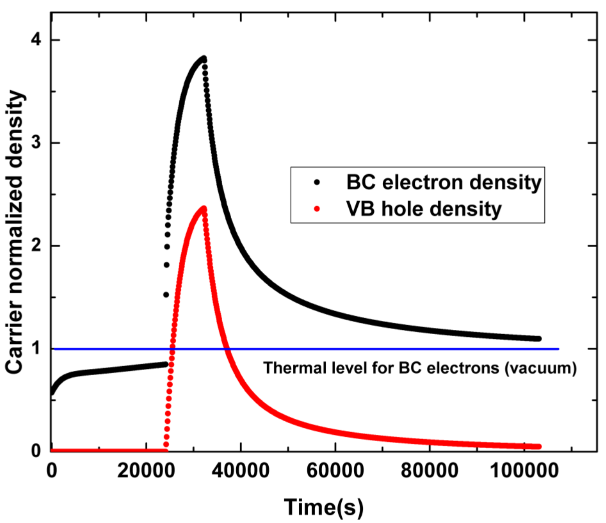

FIG. 6. Variation of carrier concentration. CB electron normalized concentration in black and VB hole normalized concentration in red.

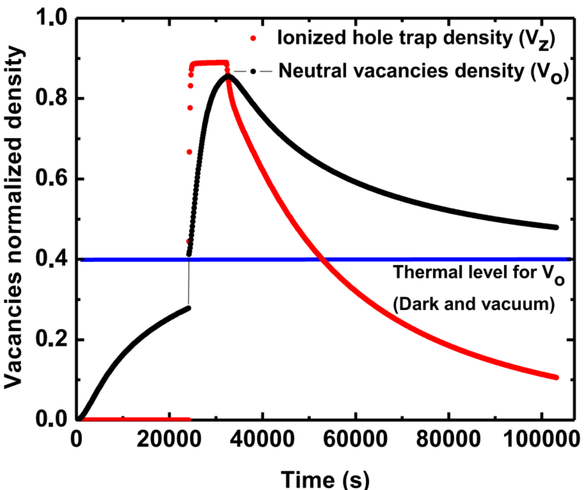

FIG. 7. Variation of ionized hole traps $V_z(t)$ and neutral vacancy $V_o(t)$ densities.

IV. DISCUSSION ABOUT THE SCOPE OF THE METHOD

Calculations based on our method can be used to refine the band and defect structure of a particular material and to estimate important transport parameters. Kim *et al.*[15] also make use of IEM to describe the transport coefficients of waves in one-dimensional random dielectric media considering the possibility of absorption or amplification. They obtain numerically results solving a large number of coupled algebraic equations (3720 equations for wave transport). Also, they argued that the method is applicable to the electron transport problem in disordered quasi-one-dimensional solids. However, the several processes of photogeneration, recombination, electron and hole capture and release by impurities, described in this work, are hard to take into account considering Kim's procedure. On the other hand, the standard method for obtaining information on photoconductivity curves is the adjustment that uses sum of time-dependent exponentials. This method is purely phenomenological and, therefore, the microscopic causes of the measured changes remain veiled, which hinders the physical interpretation of the transport processes and the characterization of the material. A limitation of our method is that the equations of the transport coefficients are valid as long as the carrier concentration does not change appreciably during the time interval used as an iteration step. In the present work, we have applied the equations to a sample whose conductivity changes a maximum of 5 times. Also, it was

Published under license by AIP Publishing.

assumed that the temperature of the sample is constant during the experiment, considering that the Joule effect is negligible. However, if the Joule effect were not negligible, this variation can be included in the equations.

V. CONCLUSIONS

In this work, we propose a method to describe the macroscopic nonsteady transport of particles through a material as a transmission problem. We use the Invariant Embedding Method to obtain a set of analytical expressions for the coefficients of transmission, generation, and absorption of particles. We apply this method to evaluate the electrical transport on a ZnO microwire with persistent photoconductivity. From a proposed energy band scheme for the microwire, we successfully fitted the time variation of the conductivity of the three stages: pre-excitation, excitation, and recuperation. This allowed us to obtain 15 parameters related to deoxidation of the surface; concentration of neutral and ionized traps; capture probabilities of the traps; photocarrier generation efficiency; ionization efficiency of different defects; electron–hole mobility relation; the probability of e-h recombination, and density of states at BC and VB. Using these parameters, we can obtain the recombination cross section of electrons and holes and capture cross sections of defects for electrons and holes. Also, this method allowed us to evaluate the time variation of the concentration of carriers in the bands and the variation of the concentration of neutral and ionized defects. All these make the proposed procedure a useful tool for verifying semiconductor band structure models and for characterizing a material from nonsteady electrical transport measurements.

ACKNOWLEDGMENTS

We thank G. Simonelli, P. Esquinazi, and D. Comedi for fruitful discussions. This work was supported by SCAIT (No. E653CX), CONICET (No. PIP 585), PICT (No. 2016-3356), and SNMAG Facility.

REFERENCES

[1] J. Noolandi, Phys. Rev. B **16**, 4474 (1977).
[2] O. L. Curtis and J. R. Srour, J. Appl. Phys. **48**, 3819 (1977).
[3] N. Schüler, T. Hahn, S. Schmerler, S. Hahn, K. Dornich, and J. R. Niklas, J. Appl. Phys. **107**, 064901 (2010).
[4] H. G. Grimmeiss and L. Ledebo, J. Appl. Phys. **46**, 2155 (1975).
[5] H. B. DeVore, Phys. Rev. **102**, 86 (1956).
[6] B. Ullrich and H. Xi, in *Optoelectronics—Advanced Materials and Devices* (InTech, 2013).
[7] A. Kolmakov and M. Moskovits, Annu. Rev. Mater. Res. **34**, 151 (2004).
[8] V. Ambarzumian, *Theoretical Astrophysics* (Pergamon Press, 1958).
[9] S. Chandrasekhar, *Radiative Transfer* (Dover Publications, 1960).
[10] R. Bellman, R. Kalaba, and G. M. Wing, J. Math. Phys. **1**, 280 (1960).
[11] G. M. Wing, *Introduction to Transport Theory* (John Wiley and Sons, 1963).
[12] K. Kim, Phys. Rev. B **58**, 6153 (1998).
[13] L. G. Glazov and I. Pázsit, Nucl. Instrum. Methods Phys. Res. Sect. B **256**, 638 (2007).
[14] C. Figueroa, H. Brizuela, and S. P. Heluani, J. Appl. Phys. **99**, 044909 (2006).
[15] K. Kim, F. Rotermund, and H. Lim, Phys. Rev. B **77**, 024202 (2008).
[16] R. Landauer, IBM J. Res. Dev. **1**, 223 (1957).
[17] M. Villafuerte, D. J. Zamora, G. Bridoux, J. M. Ferreyra, M. Meyer, and S. P. Heluani, J. Appl. Phys. **121**, 064501 (2017).
[18] K. Moazzami, T. E. Murphy, J. D. Phillips, M. C.-K. Cheung, and A. N. Cartwright, Semicond. Sci. Technol. **21**, 717 (2006).
[19] O. Schmidt, P. Kiesel, C. G. V. de Walle, N. M. Johnson, J. Nause, and G. H. Döhler, Jpn. J. Appl. Phys. **44**, 7271 (2005).
[20] O. Schmidt, A. Geis, P. Kiesel, C. G. V. de Walle, N. M. Johnson, A. Bakin, A. Waag, and G. H. Döhler, Superlattices Microstruct. **39**, 8 (2006).
[21] P. Erhart, A. Klein, and K. Albe, Phys. Rev. B **72**, 085213 (2005).
[22] M. Villafuerte, J. M. Ferreyra, C. Zapata, J. Barzola-Quiquia, F. Iikawa, P. Esquinazi, S. P. Heluani, M. M. de Lima, and A. Cantarero, J. Appl. Phys. **115**, 133101 (2014).
[23] N. C. Vega, O. Marin, E. Tosi, G. Grinblat, E. Mosquera, M. S. Moreno, M. Tirado, and D. Comedi, Nanotechnology **28**, 275702 (2017).
[24] G. Grinblat, F. Bern, J. Barzola-Quiquia, M. Tirado, D. Comedi, and P. Esquinazi, Appl. Phys. Lett. **104**, 103113 (2014).
[25] C.-Y. Chen, J. R. D. Retamal, I.-W. Wu, D.-H. Lien, M.-W. Chen, Y. Ding, Y.-L. Chueh, C.-I. Wu, and J.-H. He, ACS Nano **6**, 9366 (2012).
[26] Q. Chen, H. Ding, Y. Wu, M. Sui, W. Lu, B. Wang, W. Su, Z. Cui, and L. Chen, Nanoscale **5**, 4162 (2013).
[27] B. Straube, G. Bridoxu, C. Zapata, J. M. Ferreyra, M. Villafuerte, G. Simonelli, P. Esquinazi, C. R. Torres, and S. P. Heluani, Phys. Status Solidi B **255**, 1800056 (2018).
[28] A. Janotti and C. G. V. de Walle, Rep. Prog. Phys. **72**, 126501 (2009).
[29] M. Newville, T. Stensitzki, D. B. Allen, and A. Ingargiola, *Lmfit: Non-Linear Least-Square Minimization and Curve-Fitting for Python* (Zenodo, 2014).
[30] W. Göpel and U. Lampe, Phys. Rev. B **22**, 6447 (1980).
[31] C. H. Henry, H. Kukimoto, G. L. Miller, and F. R. Merritt, Phys. Rev. B **7**, 2499 (1973).
[32] D. V. Lang and R. A. Logan, Phys. Rev. Lett. **39**, 635 (1977).

Published under license by AIP Publishing.